ELECTRON DENSITY PROFILE OF TWO-DIMENSIONALLY CRYSTALLINE MEMBRANOUS CYTOCHROME *c* OXIDASE AT LOW RESOLUTION

UMA JAYARAMAN, TAN CHANG, T. G. FREY, AND J. K. BLASIE
Departments of Chemistry and Biochemistry and Biophysics, University of Pennsylvania, Philadelphia, Pennsylvania 19104

ABSTRACT Unilamellar vesicles of membranous cytochrome *c* oxidase have been isolated whose distribution of protein in the membrane plane was predominantly crystalline. The vesicles were collapsed via controlled partial dehydration, resulting, at first, in the formation of unoriented, mostly unstacked, membrane pairs. Further controlled partial dehydration resulted in the formation of oriented multilayers of stacks of membrane pairs, retaining the in-plane crystallinity. The above were monitored by electron microscopy and x-ray diffraction. Analysis of the x-ray diffraction from unoriented, unstacked membrane pairs by two independent methods provided the membrane electron density profile to 30 Å resolution.

INTRODUCTION

Cytochrome *c* oxidase transfers reducing equivalents from reduced cytochrome *c* to molecular oxygen in mitochondrial respiration; this reaction is normally coupled to the synthesis of ATP. The active redox components of cytochrome oxidase are two heme *a* groups and two copper atoms (for recent reviews see references 1 and 2). The Mitchell hypothesis requires that the coupling between electron transport and phosphorylation of ADP occurs via formation of an electrochemical proton gradient across the mitochondrial inner membrane (3, 4). The formation of such a proton gradient would require a specific location and orientation of cytochrome oxidase with respect to the membrane structure. The accurate determination of the positions and orientations of the oxidase redox centers relative to each other and to the membrane structure should, therefore, provide considerable insight into the nature of the electron transport and energy coupling mechanisms.

Resonance x-ray scattering effects on the x-ray diffraction arising from photon momentum transfer perpendicular to the plane of membranous cytochrome oxidase at incident x-ray energies near the respective K-absorption edges of the oxidase iron and copper atoms can provide an accurate (±1 Å) determination of the positions of the two iron atoms and the two copper atoms in membrane profile (12); this determination is considerably simplified if the low-resolution electron density profile of the membrane containing unidirectionally oriented protein was independently known for incident x-ray energies a few hundred electron volts away from the absorption edges (5–9). Previous resonance x-ray diffraction studies on reconstituted cytochrome oxidase membranes were only able to provide two pairs of possible locations for the heme *a* and a_3 iron atoms in the membrane profile primarily because the protein orientation was nearly bidirectional (see 5–7 vs. 9).

Since reconstituted membranes with nearly unidirectional protein orientation (including cytochrome oxidase) seem to be notoriously difficult to prepare and assay reproducibly for high protein contents (5), we turned to the isolation of predominantly unilamellar vesicles of two-dimensionally crystalline, membranous cytochrome oxidase because their protein orientation was known to be unidirectional based on both the crystallographic space group and subunit-specific antibody binding (10, 11, 18). These swollen unilamellar vesicles in wet pellets were collapsed via controlled, slow partial dehydration to form initially ensembles of unoriented, predominantly unstacked membrane pairs and ultimately oriented multilayers. The former specimens provided the better system for the determination of the required membrane electron density profile in a more hydrated, less densely packed state via x-ray diffraction.

METHODS

(*a*) Preparation

Dispersions containing both unilamellar and multilamellar vesicles of two-dimensionally crystalline, membranous cytochrome oxidase were prepared from beef heart mitochondria as described by Frey et al. (11).

Dr. Frey's present address is Department of Biology, San Diego State University, San Diego, CA 92182

(b) Separation of Unilamellar Vesicles

Vesicular dispersions (*a*) were diluted 2:1 with 10 mM phosphate, and 0.25 M sucrose buffer, pH 7.2. These were layered on top of a continuous sucrose density gradient consisting of 20–50% (wt/vol) sucrose and centrifuged at 9,500 rpm for 1 h (rotor model SW25; Beckman Instruments, Inc., Fullerton, CA). Two main bands were obtained at ~23 and 46% sucrose. The vesicles in the upper diffuse band were collected. These were washed via centrifugation (30,000 rpm for 1/2 h) in the sucrose phosphate buffer, homogenized, frozen in liquid nitrogen, and stored in aliquots at −80°C.

(c) Partial Dehydration

Pellets containing ~2.0 mg protein were formed by sedimenting the washed dispersion of the unilamellar vesicles (*b*) onto aluminum foil in a sedimentation cell at 22,000 rpm for 1 h. The wet pellets, ~5 mm in diameter and 0.5–1 mm thick, were attached to a cylindrically curved glass support in a cold room (3–5°C). Slow partial dehydration of the pellets was carried out at 5°C over a saturated salt (K_2SO_4) solution at 98% relative humidity in closed containers.

(d) Negative Staining

The vesicular dispersions (~0.1 mg protein/ml) from *a* and *b* were applied to carbon coated grids, made hydrophilic by glow discharging, and negatively stained with 1% (wt/vol) uranyl acetate.

(e) Thin Sections

Membrane pellets partially dehydrated for various periods of time (see *c* above) were prefixed at 5°C and 98% relative humidity for 12–18 h in glutaraldehyde vapor above the saturated salt solution and a 3.5% solution of glutaraldehyde. Then, the partially dehydrated (or in some instances wet) pellets were fixed using 1% tannic acid and 3.5% glutaraldehyde in 0.1 M cacodylate buffer (pH 7.2) for 1 h. This was followed by washing with cacodylate buffer and post fixation in 1% OsO_4 in 0.05 M phosphate buffer (pH 7.0) for 1 h. After being washed with the phosphate buffer, they were stained in 6% saturated uranyl-acetate for 90 min (13).

Total dehydration was then carried out by a graded (75–100%) ethanol series. Embedding was done in Spurr's resin. We found Epon to be unsuitable, as this more viscous resin could not penetrate the densely packed membranes to any appreciable extent.

Thin sections were cut on an ultratome with glass and diamond knives. The sections were cut parallel to the sedimentation axis of the pellets. All the sections were post-stained with lead citrate and examined in a Phillips 400T electron microscope.

(f) X-ray Diffraction

Ni filtered Cu Kα ($\lambda \simeq 1.54$ Å) x-rays were produced by a rotating anode generator (Elliott GX6; Marconi Avionics Ltd., Borhamwood, England) (29 kV × 20 mA) and line-focused at the detector entrance window via single mirror Franks' optics (14). The specimen chamber was a well sealed brass cannister with Mylar windows containing cups of the saturated salt solution and maintained at 5°C (see *c* above). The cylindrically curved membrane pellets were positioned so as to intersect the x-ray beam at grazing incidence with the line-focus parallel to the specimen surface. The diffraction patterns were recorded every half hour using a linear position-sensitive detector and a helium-filled scattered beam tube. The resolution of the x-ray optics-detector system was $\Delta s \simeq 0.0024$ Å^{-1} where $s \equiv (2 \sin \theta)/\lambda$ is the photon momentum transfer vector. A typical data set contained the sum of six to eight such records, i.e., a cumulative exposure of 3–4 h. Data collection was started soon after formation of the wet membrane pellets and was constantly monitored and recorded during the partial dehydration of the membrane pellets as the observable diffraction evolved from a single very broad peak to three broad peaks to three sharp peaks over the range ~ 0.0097 Å$^{-1} \leq s \leq \sim 0.029$ Å^{-1}.

X-ray films (Eastman Kodak Co., Rochester, NY) were also used to record the low angle lamellar and equatorial diffraction patterns at grazing and normal incidence to the specimen surface, respectively, from oriented multilayers resulting from partial dehydration for > 24 h at 5°C at 98 or 96% relative humidity. The films were contained in a flat cassette at a specimen-to-film distance of 250 mm. The exposure times were, typically, 12 h (lamellar) and 30 h (equatorial). The specimen chamber was flushed with helium at the appropriate relative humidity and the path of the x-rays was in vacuum.

RESULTS

I. Nature and Evolution of the Membrane Pellets during the Partial Dehydration

The following "typical" results were obtained for three separate preparations of unilamellar vesicles from two different preparations of two-dimensionally crystalline, membranous cytochrome oxidase as described in the Methods section *a* and *b*. The examination of the membrane pellets by thin-section electron microscopy utilized no less than three to four pellets for each of the stages of partial dehydration described below. The examination of the membrane pellets by x-ray diffraction utilized no less than five to six pellets, each studied throughout the evolution of the partial dehydration process as described below.

(a) Wet Pellets. Fig. 1 is an electron micrograph of typical thin sections of wet pellets made from the lighter fraction obtained via sucrose density gradient centrifugation. It exhibits primarily numerous swollen unilamellar vesicles of varying sizes. There are only occasional examples of a vesicle within a vesicle, the dominant feature being the unilamellar vesicles. Many of these unilamellar vesicles are two-dimensionally crystalline in the membrane plane as demonstrated by the electron microscopy of negatively stained unilamellar vesicular dispersions (Fig. 1, *inset*) and of rapidly frozen and fractured wet pellets (18). The x-ray diffraction from these wet pellets composed mostly of swollen unilamellar vesicles shows a single, very broad peak over the range ~ 0.0097 Å$^{-1} \leq s \leq \sim 0.029$ Å^{-1}, where $s \equiv (2 \sin \theta)/\lambda$ is the photon momentum transfer vector. The diffracted intensity $I_m(s)$ expected from an ensemble of swollen, unilamellar vesicles of variable diameter is generally a continuous, relatively slowly varying function of s dominated by

$$I_m(s) \alpha |F_m(s)|^2/s^2,$$

where

$$F_m(s) \overset{FT}{\longleftrightarrow} \rho_m(z).$$

$I_m(s)$ is then the spherically averaged modulus squared of the structure factor $F_m(s)$ for the electron density profile

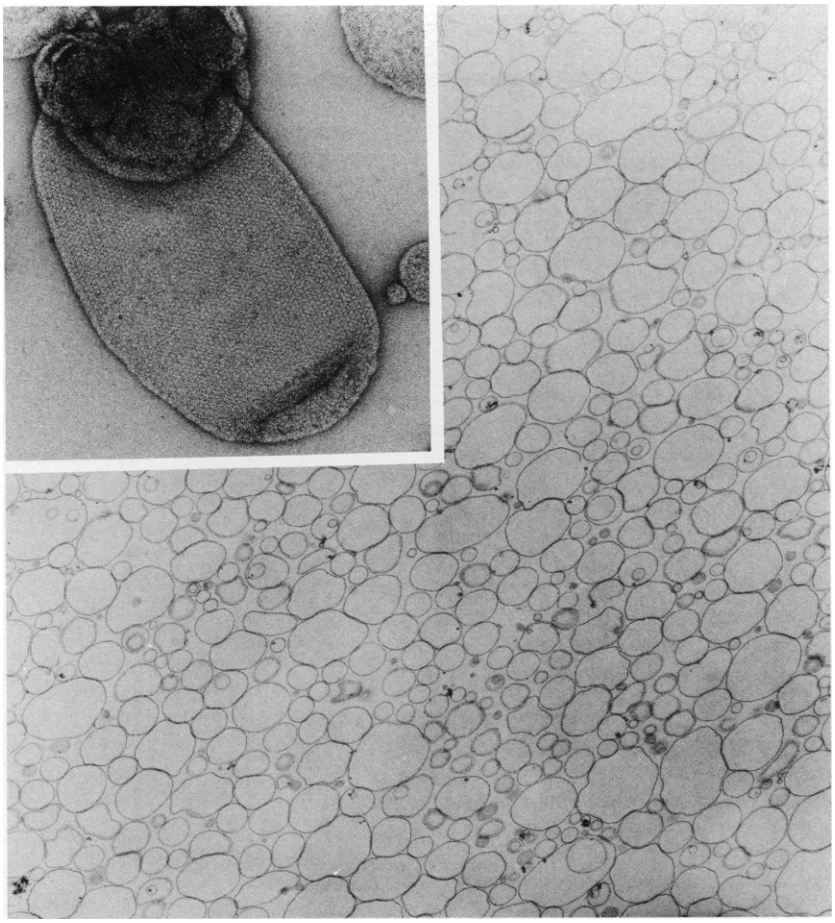

FIGURE 1 An electron micrograph (magnification 1.8×10^4) of a thin section (~400 Å) of a wet pellet of the membranous cytochrome oxidase, fixed and stained, etc. as described. The preparation consists primarily of unilamellar vesicles with a large variation in their diameters (~0.1–1 μm). There are only a few cases of vesicles within a vesicle and no multilamellar (or "onion-skin") type of vesicles can be seen. (*Inset*) An electron micrograph (magnification 1.7×10^5) of a two-dimensionally crystalline patch of cytochrome oxidase molecules on one of the unilamellar vesicles from the same vesicular dispersion obtained by negative staining as described.

$\rho_m(z)$ of a single membrane; $F_m(s)$ and $\rho_m(z)$ are simply related by a continuous, one-dimensional Fourier transform (FT). The one, very broad maximum observed in the x-ray diffraction from the wet pellets is, therefore, most likely the first observable maximum in $|F_m(s > 0)|^2$ due to diffraction from unoriented, unstacked single membrane profiles consistent with the electron microscopy results.

(b) Early Stages of Partial Dehydration. The electron micrograph in Fig. 2 shows a typical thin section of membrane pellets relatively soon (a few hours) after the partial dehydration process starts. The partially collapsed unilamellar vesicles form membrane pairs along the collapsed sections and occasionally begin to stack up. There does not seem to be any significant formation of multilamellar vesicles. Among the circled areas, two kinds of pairs can be discerned (*a*) between the membranes of one unilamellar vesicle (intravesicular) and (*b*) between the adjacent membranes of neighboring vesicles (intervesicular). There are examples where a single vesicle forms both the types of pairs along different parts of its length. At this early stage of partial dehydration, unoriented, unstacked single membranes and two types of membrane pairs constitute the specimen.

(c) Intermediate Stages of Partial Dehydration. After partial dehydration for 10–12 h or so, the pellets consist predominantly of unoriented membrane pairs with some stacking, as shown by a typical thin-section electron micrograph in Fig. 3. The x-ray diffraction arising from these pellets partially dehydrated for 10–12 h composed of unoriented, mostly unstacked, membrane pairs is shown in Fig. 5 and consists of three broad peaks over the same range of s (~ 0.0097 Å$^{-1} \leq s \leq \sim 0.029$ Å^{-1}) centered at the positions $s \sim 0.0109$, 0.0188, and 0.0279 Å^{-1}. The second maximum is the strongest in all the specimens examined; the relative intensities of the first and third peaks vary, depending on the relative amount of stacked pairs present (see Section IIc below). The diffracted intensity $I_{mp}(s)$ expected from an ensemble of unstacked, unoriented

FIGURE 2 An electron micrograph (magnification 6.6 × 10^4) of a thin section of a glutaraldehyde vapor-fixed cytochrome oxidase membrane pellet in the early stages of partial dehydration. Many partly collapsed or partly swollen unilamellar vesicles can be seen. Some have formed "uniformly" spaced paired membranes and a few of these pairs are stacked. Both types (inter- and intravesicular) of pairs are present (e.g., within the circled areas).

membrane pairs of collapsed unilamellar vesicles is again a continuous, but more rapidly varying function of s (as compared with a above), with the larger maxima at $s \sim n/a$, where $n = 1, 2, 3$, etc. and $a \simeq$ the average separation of the centers of mass of the membranes in the pair. The form of the diffraction is generally dominated by a series of $\cos^2$ and $\sin^2$ fringes modulated respectively by the symmetric and antisymmetric parts of the modulus squared of the structure factor of a single membrane, i.e.,

$$|F_{mp}(s)|^2 \propto |F_{ms}(s)|^2 \cos^2(\pi as) + |F_{ma}(s)|^2 \sin^2(\pi as) \quad (1)$$

where

$$F_{mp}(s) \overset{FT}{\longleftrightarrow} \rho_{mp}(z).$$

and

$$I_{mp}(s) \propto |F_{mp}(s)|^2/s^2. \quad (2)$$

$F_{mp}(s)$ is the structure factor for the profile of the membrane pair $\rho_{mp}(z)$; $F_{ms}(s)$ and $F_{ma}(s)$ are the symmetric and antisymmetric parts of the structure factor of a single membrane profile, $\rho_m(z)$, respectively. The approximately periodic diffraction maxima in $I_{mp}(s)$ then arise due to spherically averaged interference effects within membrane pairs exhibited through the cosine and sine terms in Eq. 1. Thus the three broad diffraction maxima observed on controlled partial dehydration of wet pellets for 10–12 h most likely originate from randomly oriented membrane pair profiles. The dominance of randomly oriented membrane pairs in these specimens is further supported by the electron microscopy on thin sections of the same pellets vapor-fixed under otherwise equivalent conditions immediately after the x-ray exposure.

(d) Final Stage of Partial Dehydration. 24 h or more of slow partial dehydration results in the dense stacking of membranes to form oriented multilayers of very evenly spaced membranes, as shown by a typical thin-section electron micrograph in Fig. 4 *A* at the end-

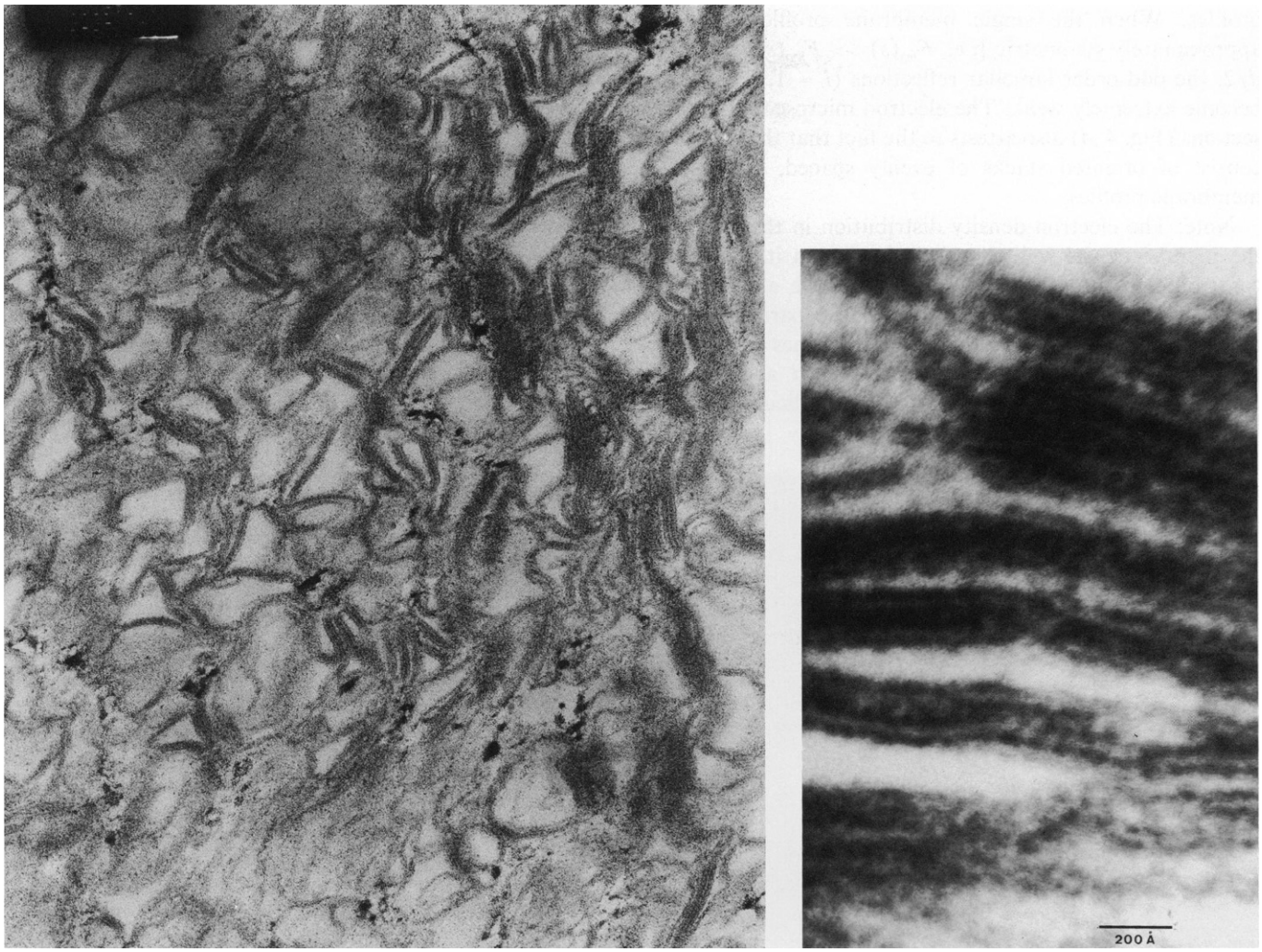

FIGURE 3 (*Left*) An electron micrograph (magnification 1.38×10^5) of an oxidase membrane pellet, vapor-fixed, at an intermediate stage of the partial dehydration process. The specimen consists predominantly of unoriented membrane pairs with some cases of stacked membrane pairs. The figure shown is a thin section of such a pellet, glutarldehyde vapor-fixed immediately after an x-ray exposure. (*Right*) A higher magnification (1.0×10^6) electron micrograph of a few membrane pairs. The total profile width of the pairs evident in the electron image is ~200 Å.

point of such progressive partial dehydration of these membrane pellets. Fig. 4 *B* shows the lamellar diffraction at grazing incidence from typical pellets partially dehydrated for ~24 h composed of an oriented multilayer of stacked membrane pairs. Only the even order, sharp reflections for $l = 2, 4$, and 6 are present where $s = 2\sin\theta/\lambda = l/d$ and $d \simeq 188$ Å is the multilayer periodicity along z; no equatorial reflections due to in-plane crystalline order can be seen for this beam incidence. Fig. 4 *C* shows the equatorial diffraction from the same oriented multilayer at normal incidence. The (h, k, l) reflections (1, 1, 0) and (0, 2, 0) are due to the in-plane crystalline order (10, 19) for a $p22_12_1$ lattice with planar unit cell dimensions $a \simeq 102$ Å, $b \simeq 134$ Å. Quite strong lamellar orders (0, 0, 2) and (0, 0, 4) can also be seen due to the relatively large mosaic spread, i.e., layer misorientation (15), of these multilayer specimens. Both the lamellar and equatorial diffraction from these oriented multilayers have been observed simultaneously utilizing grazing incidence and a point-focused incident x-ray beam. The meridional diffracted intensity from a multilayer composed of oriented stacks of flattened, unilamellar vesicles should contain a periodic series of sharp lamellar reflections at $s = l/d$, which sample the modulus squared of the structure factor for the membrane pair profile:

$$I_{ML}(s) \propto |F_{mp}(s)|^2 \cdot Z(s), \tag{3}$$

where $Z(s)$ is the interference or sampling function, which is nonzero only at $s = l/d$ for l integer and d the multilayer periodicity along z. The three discrete reflections observed on film on further partial dehydration (Fig. 4 *B*) of the membrane pellets for 24 h or more are therefore most likely the even order lamellar reflections ($l = 2$, 4, and 6; $d \simeq 188$ Å) from an oriented multilayer of membrane pair

profiles. When the single membrane profile $\rho_m(z)$ is approximately symmetric [i.e., $F_{ms}(s) >> F_{ma}(s)$] and $a \simeq d/2$, the odd order lamellar reflections (l = 1, 3, 5, etc.) become extremely weak. The electron microscopy on thin sections (Fig. 4 *A*) also attests to the fact that these pellets consist of oriented stacks of evenly spaced, symmetric membrane profiles.

Note: The electron density distribution in the plane of the membrane, as well as perpendicular to it, can both contribute to the diffracted intensity in the above cases (*a–c*); these two contributions cannot be separated in the diffraction from unoriented single membranes and membrane pairs. However, in our case (see *d* above), the contribution from the distribution perpendicular to the membrane plane or membrane profile evidenced by the (0, 0, l) lamellar reflections from oriented multilayers is considerably larger than from that in the membrane plane as evidenced by the (h, k, 0) equatorial reflections from oriented multilayers.

II. Determination of the Membrane Electron Density Profile for Unoriented Membrane Pairs

The meridional lamellar x-ray diffraction from oriented multilayers formed from predominantly unilamellar, two-dimensionally crystalline vesicles of membranous cytochrome oxidase always contained only the even order

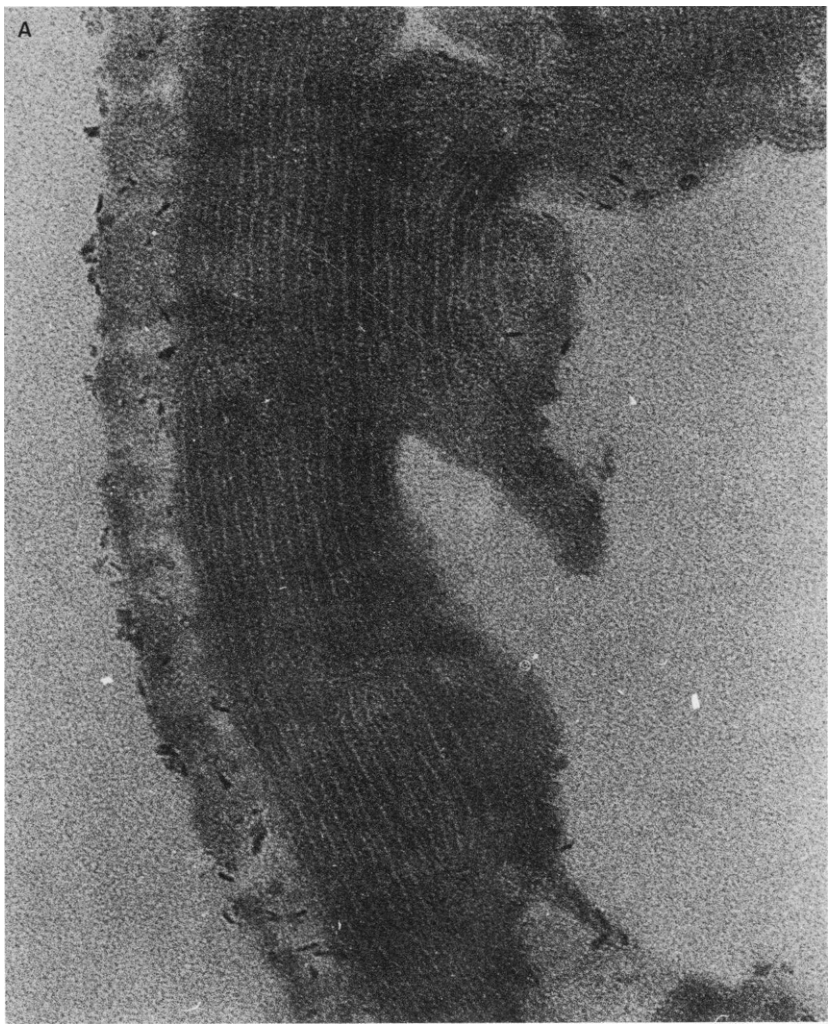

FIGURE 4 An electron micrograph (*A*) (magnification 4.86 × 10^5) of a thin section (~800 Å) of an oxidase membrane pellet at the final stage of partial dehydration (rel. hum. 98%, 5°C), namely an oriented multilayer of oxidase membranes sectioned in a plane parallel to the sedimentation axis. A unit cell in the multilayer profile containing a pair of these very evenly spaced membrane profiles has a dimension of ~180 Å. (*B*) shows the low-angle, meridional lamellar x-ray diffraction arising from these oriented multilayers. Only the sharp, even order reflections (0, 0, l) for l = 2, 4, and 6 are present for a multilayer profile periodicity of $d \simeq$ 188 Å. (*C*) shows the low-angle (same specimen-to-film distance as in *A*) equatorial x-ray diffraction taken at normal incidence to the multilayer surface using a line-focused beam. The equatorial (h, k, 0) reflections evident are indexed (1, 1, 0) and (0, 2, 0) for a $p22_12_1$ lattice with planar unit cell dimensions $a \simeq$ 102 Å, $b \simeq$ 134 Å, and occur between the second and fourth lamellar orders, (0, 0, 2) and (0, 0, 4), evident due to the mosaic spread (layer misorientation) of these multilayers.

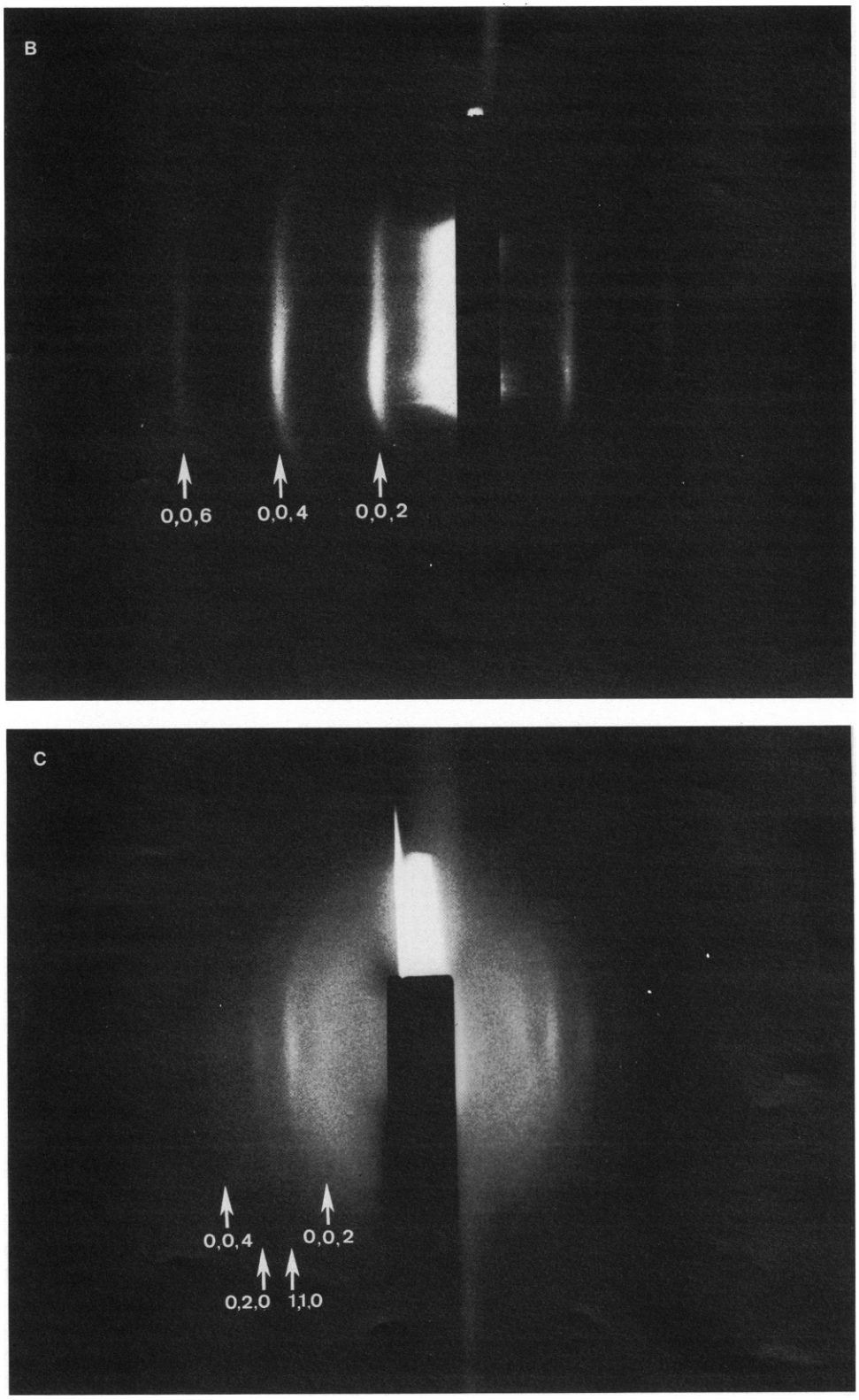

FIGURE 4 Continued.

reflections for $l = 2, 4, 6$ and sometimes $l = 8$ and $d \simeq 188$ Å (Fig. 4 *B*). Not once were we able to observe any odd orders from these partially dehydrated, oriented membrane multilayers. This can occur when the single membrane profile $\rho_m(z)$ is nearly symmetric in the multilayer [then $F_{ms}(s) >> F_{ma}(s)$ in Eq. 1 and $a \simeq d/2$]. The electron micrographs of thin sections parallel to the sedimentation axis show very evenly spaced and densely packed symmetric membrane profiles. In the absence of significant amounts of multilamellar (or "onion skin") type vesicles in the membrane pellets investigated, it would appear therefore that if the single membrane profiles are indeed asymmetric in the ensembles of unoriented, unstacked membrane pairs in more hydrated pellets, they must have become symmetric in the less hydrated, densely packed oriented multilayers. This could occur as the collapsed vesicles come very close together to form densely packed multilayers via substantial interdigitation of protein protruding from the apposed surfaces of adjacent membranes leading to the apparent symmetrization of the average single membrane profile (20). Therefore, we chose to analyze the x-ray diffraction data from the ensemble of unoriented, unstacked membrane pairs contained in less densely packed membrane pellets of higher water content for the determination of the profile structure of the cytochrome oxidase membrane in a more natural state, at least for lower-spatial resolution.

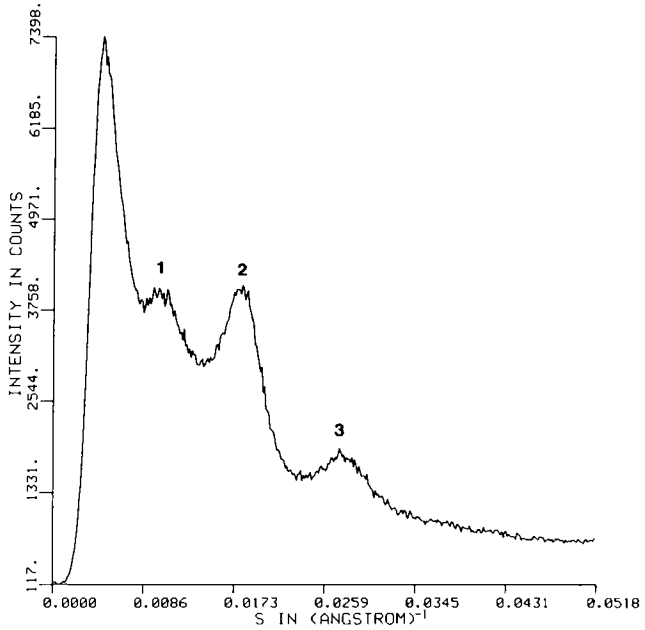

FIGURE 5 The x-ray diffraction pattern from oxidase membrane pellets at an intermediate stage of partial dehydration containing predominatly unoriented, unstacked membrane pairs, obtained by the flattening of two-dimensionally crystalline, unilamellar vesicles during the slow partial dehydration process. The diffraction maxima indexed as $n \simeq 1$, 2, and 3 (see text) are evident in this 3½ h exposure. The diffracted intensity is plotted in total x-ray counts vs. $s(\text{Å}^{-1})$.

(a) X-ray Diffraction Data Reduction. A correction for background scattering was applied to the observed total diffracted intensity data from pellets consisting predominantly of an ensemble of unstacked, unoriented membrane pairs (e.g., Fig. 5). Straight line segments were fitted between each pair of adjacent minima on either side of each of the three maxima in the logarithm of the diffracted intensity. The difference between these straight line segments (piece-wise continuous) and the logarithm of the diffracted intensity was taken as the logarithm of the background scattering-corrected diffracted intensity function $I(s) \sim I_{mp}(s)$. The background scattering-corrected intensity functions were further corrected by a factor of s^2 allowing for the spherical averaging of the unoriented membrane pair profiles to provide $s^2I(s) \sim |F_{mp}(s)|^2$.

(b) Comment on the Patterson Function. The generalized Patterson function $Q(z)$ can be calculated by an integral Fourier transform of the corrected intensity function.

The Patterson function $Q(z)$ for an ensemble of swollen unilamellar vesicles is then given by

$$|F_m(s)|^2 \overset{FT}{\longleftrightarrow} Q(z) = \rho_m(z) * \rho_m(-z) \equiv Q_m(z),$$

where * denotes the convolution operation. Thus, $Q_m(z)$ is the autocorrelation function of a single membrane profile. For a membrane profile of thickness m, $Q_m(z)$ extends from $-m \leq z \leq +m$.

For an ensemble of unoriented membrane pairs with an average separation of the centers of mass of the membranes in the pair of a, the Patterson function $Q(z)$ is then

$$|F_{mp}(s)|^2 \overset{FT}{\longleftrightarrow} Q(z) = \rho_{mp}(z) * \rho_{mp}(-z) \equiv Q_{mp}(z),$$

$Q_{mp}(z)$, the autocorrelation of the membrane pair profile, is nonzero only in the interval $-(a + m) \leq z \leq +(a + m)$.

The Patterson function $Q(z)$ for oriented multilayers is then

$$|F_{mp}(s)|^2 \cdot Z(s) \overset{FT}{\longleftrightarrow} Q(z)$$

$$= [\rho_{mp}(z) * \mathrm{r}_{mp}(-z)] * \tilde{l}^2(z) \equiv Q_{ML}(z),$$

where $\tilde{l}^2(z)$, the multilayer lattice autocorrelation function, is at least pseudo-periodic in the multilayer periodicity d depending on the nature of disorder in the multilayer lattice (16).

(c) Experimental Membrane Pair Patterson Function. A typical experimental Patterson function $Q_e(z) \sim Q_{mp}(z)$ obtained by Fourier transformation of the fully corrected intensity functions $s^2I(s) \sim |F_{mp}(s)|^2$ for pellets consisting predominantly of unstacked, unoriented membrane pairs is shown in Fig. 6. The largest amplitude

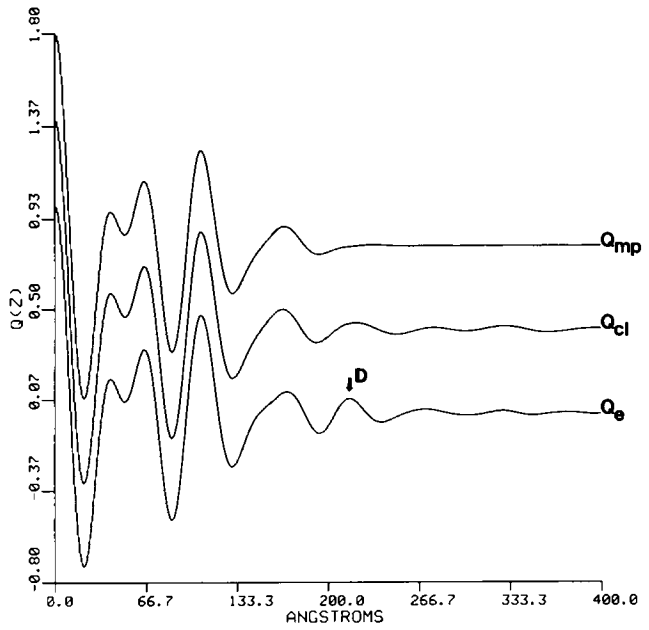

FIGURE 6 Patterson functions $Q(z)$ generated by the GFSDM analysis of the x-ray diffraction from membrane pellets at an intermediate stage of partial dehydration, namely ensembles of randomly oriented, unstacked membrane pairs. Q_e is the experimental Patterson function and "Q_{cl}" is the calculated $Q_{ML}(z)$ function, respectively. Q_{cl} was calculated for the phase combination + − + for the three diffraction maxima for $n \simeq 1, 2,$ and 3 of Fig. 5; D = 218 Å and γ = 32 Å. Q_{mp} is strictly the calculated autocorrelation of the membrane pair profile, $\rho_{mp}(z) * \rho_{mp}(-z)$, for this phase combination.

nonorigin peak, which is about half the height of the origin peak, occurs at $z \simeq 108$ Å. It arises from the strong correlations between the two membrane profiles in the pair over the distance $z \simeq a$. For $z \geqslant a$, the features in $Q_{mp}(0 \leqslant z \leqslant a)$ are repeated, though attenuated by a factor of ~2 and somewhat broadened in $Q_{mp}(a \leqslant z \leqslant a + m)$, where $(a + m) \simeq 200$ Å, as expected. The small amplitude maximum at $z \simeq 218$ Å is quite symmetrical, like the third, only much broader, and is due to the small amount of stacked membrane pairs present in these specimens with considerable disorder in the lattice of periodicity $d \simeq 218$ Å. For larger amounts of stacked membrane pairs present in the specimen (see below), this maximum should become progressively larger in amplitude along with those for $z > d$ as $Q_e(z) \rightarrow Q_{ML}(z)$ becoming pseudo-periodic in d. This small amplitude, broad maximum at $z \simeq 218$ Å and the vanishingly small oscillations for $z > 218$ strongly suggest that the Patterson function $Q_e(z)$ for these pellets partially dehydrated for 10–12 h is dominated almost exclusively by

$$Q_e(z) \sim Q_{mp}(z) = \rho_{mp}(z) * \rho_{mp}(-z).$$

Conversely, the large amplitude of the features in Q_e(108 Å $\leqslant z \leqslant$ 200 Å) relative to those in Q_e(0 Å $\leqslant z \leqslant$ 108 Å) clearly indicate that $Q_e(z)$ contains little contribution from swollen unilamellar vesicles via $Q_m(z)$.

The typical evolution of the Patterson function $Q_e(z) \rightarrow Q_{ML}(z)$ as the partial dehydration proceeds beyond 10–12 h is shown in Fig. 7. The nonorigin peak at d ~247 Å progressively sharpens and increases in amplitude along with the pattern of maxima in $Q_e(z \geqslant d)$ as the membranes stack and orient, producing a Patterson function $Q_e(z) \sim Q_{ML}(z)$ fully pseudoperiodic in d.

(d) Derivation of the Membrane Electron Density Profile. Two independent methods were used for the derivation of the membrane electron density profile $\rho_m(z)$ from the fully corrected intensity function $s^2I(s) \sim |F_{mp}(s)|^2$.

□ *(i)* GFSDM The generalized Fourier synthesis deconvolution method (GFSDM) (16) assumes centrosymmetry of the membrane pair profile structure i.e., $\rho_{mp}(z) = \rho_{mp}(-z)$. The model parameters "$\gamma$" (lattice disorder) and "d" are estimated and refined from the experimental Patterson function $Q_e(z) \sim Q_{ML}(z)$, where $Q_{ML}(z) \rightarrow Q_{mp}(z)$ for γ "large" (i.e., $\gamma \rightarrow d$). "γ", the standard deviation in d (assuming a Gaussian probability distribution), and "d" are used to calculate a model sampling function $Z(s)$. $I_{ML}(s)$ is then calculated using Eq. 3 and its Fourier transform is the calculated $Q_{ML}(z)$ function. The calculated and experimental diffracted intensity and Pat-

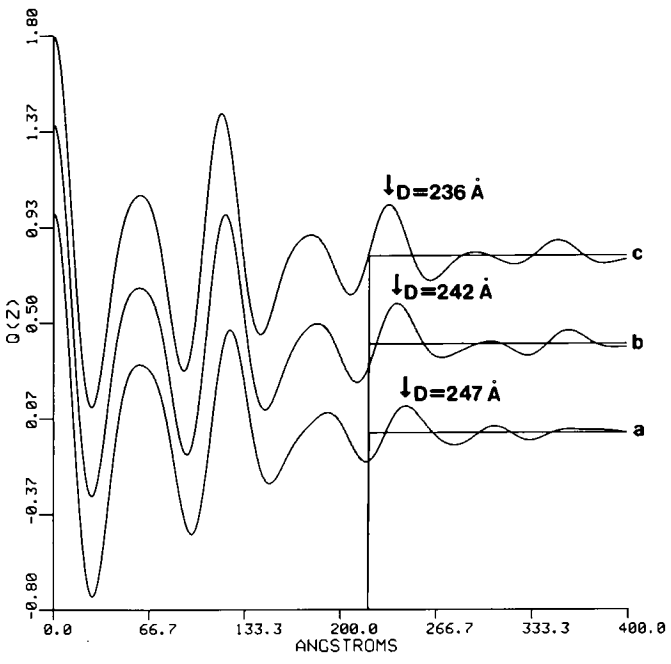

FIGURE 7 Evolution of the experimental Patterson function $Q_e(z)$ as the membrane pellets slowly dehydrate from an intermediate stage toward the final stage of partial dehydration. (*a*) The Patterson function for the most wet and (*c*) for the least wet hydration state in this series. The z-position of the peak at D, which is due to the correlation of neighboring membrane pair profiles, decreases while the peak itself sharpens and increases in amplitude as dehydration proceeds from *a* to *c*. The progressive increase in stacking of the membrane pairs is also reflected in the decrease in the related stacking disorder parameter γ. The γ values are 34, 30, and 28 Å, respectively.

terson functions are compared for all the possible phase combinations for the maxima of $F_{mp}(s) = \pm|F_{mp}(s)|$ and the best least squares fit between the calculated and experimental functions establishes the correct phase combination when γ is sufficiently large (see reference 16).

Of all the four possible phase combinations (the other four being the inverted profiles of these) the set + − + and + − − gave a much better Patterson function fit than the other two. Out of these two, + − + is consistently better for all the experimental data sets analyzed. Therefore, based on the GFSDM, the preferred membrane pair electron density profile $\rho_{mp}(z)$ is as shown in Fig. 8, corresponding to a phase change at both the minima between the three maxima in the experimental diffracted intensity function.

It was found that if the profile extent of $\rho_{mp}(z)$ was strictly taken as $-d/2 \leq z \leq +d/2 = 109$ Å, the relative amplitudes of the second and third nonorigin peaks and the shape of the fifth nonorigin peak in the calculated $Q_{mp}(z)$ and hence $Q_{ML}(z)$ did not exactly fit those in the experimental $Q_e(z)$. These peaks contain significant contributions from, respectively, the correlation of the features denoted as "X" with "Y" and "X" with "Z" in Fig. 8. Thus the relatively electron deficient trough (X) in the profile occurring at $z \sim \pm 118$ Å is an important feature in $\rho_{mp}(z)$ for the reconstruction of the correct Patterson function $Q_{ML}(z) \sim Q_{mp}(z)$, and hence a significant part of the membrane electron density profile $\rho_m(z)$.

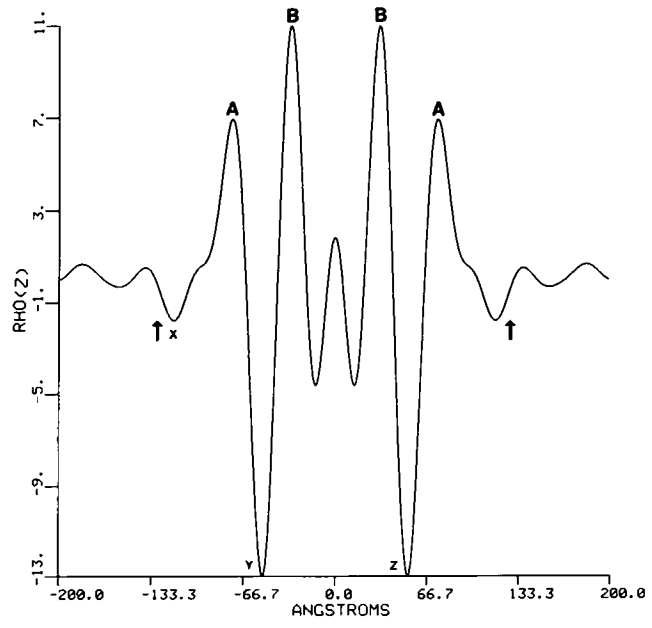

FIGURE 8 The low resolution (~30 Å) electron density profile of the membrane pair, $\rho_{mp}(z)$, derived via the GFSDM. The intramembrane phospholipid head group separation (AB) across the membrane profile $\rho_m(z)$ is ≃ 41 Å. The headgroup separation across the intravesicular water space in $\rho_{mp}(z)$ is $BB \simeq 65$ Å. The extent of the membrane pair profile $\rho_{mp}(z)$, essential for acceptable reconstruction of the Patterson function $Q_{ct}(z)$ up to $z \simeq d$, is shown by the short vertical arrows. These arrows are ~128 Å from the $z = 0$ Å origin.

□ (*ii*) BOX REFINEMENT This method (17) assumes no particular symmetry for $\rho_{mp}(z)$, unlike the GFSDM, which assumes a centrosymmetric $\rho_{mp}(z)$. It uses the amplitudes $|F_{mp}(s)|$ obtained from the experimentally determined, corrected, continuous intensity function $s^2I(s) \sim |F_{mp}(s)|^2$ along with phases from an arbitrary trial function $\rho_t(z)$ and the knowledge of the profile extent of the structure $\rho_{mp}(z)$ to refine to one of the possible phase solutions for the membrane pair electron density profile. The approximately correct profile extent of the structure $\rho_{mp}(z)$, which is the important constraint, can be provided by the value of $z = z_0$ for which $Q(z > z_0)$ becomes effectively zero. If z_0 is too small, convergence of the refinement to a reasonable phase solution is not possible. On the other hand, too large a z_0 would require many more iterations to converge to a phase solution.

Box refinement on the fully corrected intensity function $s^2I(s) \sim |F_{mp}|^2$, using a two-step or strip function model displaced from the z-origin as the trial function and the box constraint of $z_0 \sim 256$ Å, yields the solution for $\rho_{mp}(z)$ shown in Fig. 9. The number of iterations in the refinement was 10. A very similar membrane pair profile is obtained with a simple ramp function as the trial function. Box refinement provides similar results for all the experimental data sets. The apposed single membrane profiles $\rho_m(z)$ within $\rho_{mp}(z)$ agree very well with those from the GFSDM $\rho_{mp}(z)$ profile, thus strongly reinforcing the phase solution

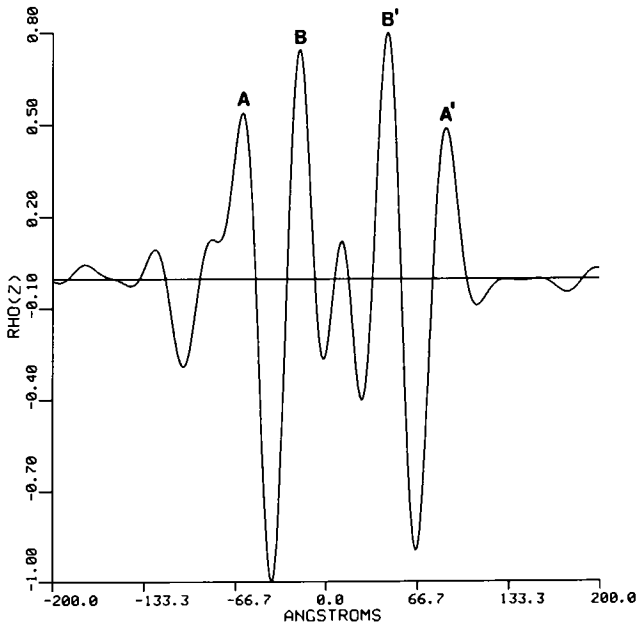

FIGURE 9 The low-resolution (~30 Å) electron density profile for the membrane pair, $\rho_{mp}(z)$ obtained by box refinement. The size of the box constraint was $z_0 \simeq 256$ Å. The trial structure was a displaced strip function being constant and nonzero only over -50 Å $< z <$ 60 Å. Some minor asymmetry in the refined $\rho_{mp}(z)$ is apparent (e.g., the relative electron density of feature $A \neq A'$, $B \neq B'$, etc.), which is somewhat dependent on the trial structure utilized. An even more symmetric refined $\rho_{mp}(z)$ can be obtained by applying pressure during the refinement iterations toward centrosymmetry as described on p. 506 of reference 17.

obtained; the refined membrane pair electron density profile obtained by box refinement can be made perfectly centrosymmetric and identical to that obtained by the GFSDM by simply subjecting $\rho_{mp}(z)$ and $\rho_{mp}(-z)$ to weighted averaging (17).

DISCUSSION

The various forms of electron microscopy performed on the unilamellar vesicles of membranous cytochrome oxidase prepared as described suggest that a large majority of these vesicles contain extensive, two-dimensionally crystalline arrays of cytochrome oxidase molecules. The x-ray diffraction studies on partially dehydrated, oriented multilayers formed from these unilamellar vesicles confirm this conclusion and further indicate that the arrays consist of a single two-dimensional lattice form.

The membrane pellets of these unilamellar vesicles of membranous cytochrome oxidase can reproducibly be made to consist predominantly of an ensemble of unoriented, unstacked membrane pairs at least transiently (several hours) during the partial dehydration process, as verified by electron microscopy and x-ray diffraction. This system of membrane pairs allows a determination of the membrane electron density profile in the absence of potential membrane modifications (21) occurring upon the formation of stable, oriented multilayers of densely packed membrane pairs including protein interdigitation between closely apposed membrane pairs (20).

The average membrane pair electron density profile $\rho_{mp}(z)$ in the ensemble of unoriented, unstacked membrane pairs arrived at by both the GFSDM and box refinement phasing methods is a pair of apposed, quite asymmetric membrane profiles, i.e., $\rho_m(z) \neq \rho_m(-z)$. This is consistent with structural studies by electron microscopy, which also indicate a similar strongly asymmetric membrane profile (10, 19). Since these specimens composed predominantly of unoriented, unstacked membrane pairs could contain both intravesicular and intervesicular types of membrane pairs as suggested by the electron microscopy, one type is obviously quite dominant; otherwise, a symmetric average membrane profile, i.e., $\rho_m(z) = \rho_m(-z)$ would have resulted. Therefore, the single membrane profile $\rho_m(z)$ is at least as asymmetric as shown, and possibly more so. The remarkably close similarity (in terms of the relative positions and asymmetry of the two apposed membrane profiles) between the derived membrane pair electron density profiles and the analogous heavy-metal stained profile from the electron microscopy (10, 19, 22) suggests that the predominant membrane pair is that formed by the collapse of the unilamellar vesicles (i.e., "intravesicular").

From the GFSDM-derived membrane electron density profile at 30 Å resolution, the oxidase protein should therefore protrude 35–44 Å beyond the membrane lipid bilayer boundary at the extravesicular surface (M-side) defined by the polar headgroup peak at $|z| \sim 74$ Å. The oxidase protein can protrude from 33–65 Å from the intravesicular surface (C-side) of the membrane lipid bilayer, defined by the polar headgroup peak at $|z| \sim 33$ Å, depending upon the extent of interdigitation of the protein molecules protruding from the apposed membrane surfaces in the intravesicular water space in $\rho_{mp}(-33 \text{ Å} \leq z \leq 33 \text{ Å})$ as indicated by the electron microscopy (10, 18). Hence, the total extension of the cytochrome oxidase molecule in the membrane profile appears to be at least 109 Å and <150 Å.

CONCLUSION

We have derived via x-ray diffraction analysis the low-resolution (30 Å) electron density profile for the membrane pair resulting from flattened, unilamellar vesicles of two-dimensionally crystalline cytochrome oxidase in the absence of heavy metals employed in electron microscopy. The more hydrated cytochrome oxidase membrane system utilized consisted of an ensemble predominantly of randomly oriented, unstacked membrane pairs, thereby avoiding membrane modifications (real or apparent) that can occur upon the dense packing of these membrane pairs in less hydrated oriented multilayers. This cytochrome oxidase membrane system is entirely suitable for resonance x-ray diffraction experiments for the accurate (±1 Å) determination of the positions of the heme *a* and a_3 iron atoms and the two copper atoms of cytochrome oxidase in the membrane profile now that a low-resolution membrane electron density profile has been unambiguously derived.

We would like to acknowledge the support of the National Institutes of Health grants HL18708 and GM33525 (to J. K. Blasie) and GM28750 (to T. G. Frey).

Received for publication 22 November 1985 and in final form 25 November 1986.

REFERENCES

1. Wikstrom, M., K. Krab, and M. Saraste. 1981. Cytochrome Oxidase: A Synthesis. Academic Press, Inc., London.
2. Capaldi, R. A., F. Malatesta, and V. M. Darley-Usmar. 1983. Structure of cytochrome *c* oxidase. *Biochim. Biophys. Acta.* 726:135–148.
3. Mitchell, P. 1961. Coupling of phosphorylation to electron and hydrogen transfer by a chemi-osmotic type of mechanism. *Nature (Lond.).* 191:144–148.
4. Mitchell, P. 1966. Chemiosmotic coupling in oxidative and photosynthetic phosphorylation. *Biol. Rev.* 41:445–502.
5. Tavormina, A. M. 1981. The utility of resonance x-ray diffraction for determining the positions of intrinsic metal atoms within biological membranes: studies on a reconstituted cytochrome *c* oxidase system. Ph.D. thesis. University of Pennsylvania, Philadelphia, PA.
6. Stamatoff, J., P. Eisenberger, J. K. Blasie, J. M. Pachence, A. Tavormina, M. Erecisnka, P. L. Dutton, and G. Brown. 1982. The location of redox centers in biological membranes determined by resonance x-ray diffraction. I. Observation of the resonance effect. *Biochim. Biophys. Acta.* 679:177–187.
7. Blasie, J. K., J. M. Pachence, A. Tavormina, M. Erecisnka, P. L. Dutton, J. Stamatoff, P. Eisenberger, and G. Brown. 1982. The location of redox centers in biological membranes determined by

resonance x-ray diffraction. II. Analysis of the resonance diffraction data. *Biochim. Biophys. Acta.* 679:188–197.

8. Blasie, J. K., and J. Stamatoff. 1981. Resonance x-ray scattering: its use in determining spatial relationships among metal atoms within macromolecules in a non-crystalline state. *Annu. Rev. Biophys. Bioeng.* 10:451–458.
9. Blasie, J. K., J. M. Pachence, A. Tavormina, P. L. Dutton, J. Stamatoff, P. Eisenberger, and G. Brown. 1983. The location of redox centers in the profile structure of a reconstituted membrane containing a photosynthetic reaction center-cytochrome *c* complex by resonance x-ray diffraction. *Biochim. Biophys. Acta.* 723:350–357.
10. Henderson, R., R. A. Capaldi, and J. S. Leigh. 1977. Arrangement of cytochrome oxidase molecules in two-dimensional vesicle crystals. *J. Mol. Biol.* 112:631–648.
11. Frey, T. G., S. H. P. Chan, and G. Schatz. 1978. Structure and orientation of cytochrome *c* oxidase in crystalline membranes. *J. Biol. Chem.* 253:4389–4395.
12. Blasie, J. K., L. Herbette, and J. M. Pachence. 1985. Biological membrane structure as "seen" by x-ray and neutron diffraction techniques. *J. Membr. Biol.* 86:1–7.
13. Herbette, L., A. Scarpa, J. K. Blasie, C. T. Wang, T. A. Saito, and S. Fleischer. 1981. Comparison of the profile structures of isolated and reconstituted sarcoplasmic reticulum membranes. *Biophys. J.* 36:47–72.
14. Franks, A. 1955. An optically focusing x-ray diffraction camera. *Proc. Phys. Soc. Lond. Sec. B.* 68:1054–1064.
15. Guinier, A. 1963. X-ray diffraction in crystals, imperfect crystals, and amorphous bodies. W. H. Freeman & Co. Publishers, San Francisco.
16. Schwartz, S., J. E. Cain, E. Dratz, and J. K. Blasie. 1975. An analysis of lamellar x-ray diffraction from disordered membrane multilayers with application to data from retinal rod outer segments. *Biophys. J.* 15:1201–1233.
17. Stroud, R. M., and D. A. Agard. 1979. Structure determination of asymmetric membrane profiles using an iterative Fourier method. *Biophys. J.* 25:495–512.
18. Frey, T. G., M. J. Costello, B. Karlsson, J. C. Haselgrove, and J. S. Leigh. 1982. Structure of the cytochrome *c* oxidase dimer. Electron microscopy of two-dimensional crystals. *J. Mol. Biol.* 162:113–130.
19. Deatherage, J. F., R. Henderson, and R. A. Capaldi. 1982. Three-dimensional structure of cytochrome *c* oxidase vesicle crystals in negative stain. *J. Mol. Biol.* 158:487–499.
20. Pascolini, D., J. K. Blasie, and S. M. Gruner. 1984. A 12 Å resolution x-ray diffraction study of the phase behavior and electron density profile of isolated bovine retinal rod outer segment disk membranes. *Biochim. Biophys. Acta.* 777:9–20.
21. Herbette, L., P. DeFoor, S. Fleischer, D. Pascolini, A. Scarpa, and J. K. Blasie. 1985. The separate profile structures of the calcium pump protein and the phospholipid bilayer within isolated sarcoplasmic reticulum membranes determined by x-ray and neutron diffraction. *Biochim. Biophys. Acta.* 817:103–122.
22. Frey, T. G., and T. Chang. 1986. The structure of membrane bound cytochrome oxidase. *Ann. NY Acad. Sci.* In press.